Journal of Materials Chemistry C

ROYAL SOCIETY OF CHEMISTRY

PAPER

View Article Online
View Journal | View Issue

Cite this: J. Mater. Chem. C, 2021, 9, 2483

Surface organic ligand-passivated quantum dots: toward high-performance light-emitting diodes with long lifetimes†

Lishuang Wang, [ab] Ying Lv, [c] Jie Lin, [c] Jialong Zhao, *[b] Xingyuan Liu,*[c] Ruosheng Zeng,[b] Xun Wang [d] and Bingsuo Zou *[b]

Received 17th November 2020,
Accepted 6th January 2021

DOI: 10.1039/d0tc05391k

rsc.li/materials-c

For quantum dot light-emitting diodes (QLEDs), typical colloidal quantum dots (QDs) are usually composed of a core/shell heterostructure which is covered with organic ligands as surface passivated materials to confine the carriers in QDs and prevent the agglomeration and growth of QDs. To enhance the electroluminescence (EL) performance of QLEDs, capping ligand modified QDs were synthesized to improve the QD passivation and stability as well as luminance efficiency. Here, short thiol-based ligands (1-dodecanethiol (DDT) and 1-octanethiol (OT)) are used to investigate the surface organic ligand effect on device performance. Moreover, the QDs with shorter OT ligands (OT-QDs) show efficient passivation and achieve high photoluminescence properties. The QLEDs based on OT-QDs achieve an improved overall charge balance in LEDs and a maximum EQE over 25%. An operational lifetime (T_{50}) over 420 000 h is obtained for OT based QLEDs, which is a 3.42-times enhancement compared to DDT based QLEDs. This work highlights the potential of thiol-based ligands for the surface passivation of QDs, for improved stability as well as performance in QLEDs.

Introduction

Due to their wide range of flexible advantages, including a performance-controllable and easily processed chemical synthesis, high photoluminescence (PL) quantum yield (QY), high photophysical stability, size-tunable high-purity emission, and convenient subsequent treatment process and integration with other devices, colloidal quantum dots (QDs) are widely used in light-emitting diodes (LEDs), laser devices, solar cells, chemical biosensors, biological imaging, and photodetectors.[1–6] In particular, for optoelectronic applications, the low-cost solution-process makes QDs one of the most interesting research hotspots.[7–9] For LEDs, typical QDs are usually made up of a core/shell heterostructure which is covered with a giant alloyed-shell and surface passivated organic ligands.[10–13] In the principle of quantum confinement effects, the synthetic refinements of the giant shell were applied in the QD structure design to minimize the nonradiative progress by engineering the size.[14,15] X. G. Peng's group paid attention to PL QY enhancement and the nonblinking QDs; the controlled thickness shells made QDs stable under ambient conditions.[16] W. K. Bae's group studied the influence of shell thickness on the performance of light-emitting diodes based on QDs (QLEDs), and they found that the shell thickness indeed suppressed the nonradiative progress and reached an improvement in device efficiency.[17,18] However, the ZnS or ZnCdS shells provide an energetic barrier for carrier injection from the transport layer into QDs. Too thick shells could cause imbalanced carrier injection and transport, and reduction of electroluminescence (EL) performance. Meanwhile, field induced quenching which is responsible for the efficiency roll-off behavior is more pronounced for thicker shells that have a typically negative effect on the operational lifetime.[19,20] Thus, an optimized strategy needs to be used to achieve high PL characteristic QDs for light-emitting devices.

To improve the photophysical properties, surface chemistry modification has long been used to achieve nonblinking, and stable QDs. The nature of surface organic ligand modification is that the ligands affect the superficial defects of QDs, leading to an enhanced carrier transport in QD thin films and improved PL QY.[21,22] By isolating QDs from neighboring ones, the ligands

[a] College of Chemistry and Chemical Engineering, Guangxi University, Nanning 530004, China
[b] MOE Key Lab of New Processing Technology for Nonferrous Metals and Materials and Guangxi Key Lab of Processing for Nonferrous Metals and Featured Materials, School of Physical Science and Technology, Guangxi University, Nanning 530004, China. E-mail: zhaojl@ciomp.ac.cn, zoubs@gxu.edu.cn
[c] State Key Laboratory of Luminescence and Applications, Changchun Institute of Optics, Fine Mechanics and Physics, Chinese Academy of Sciences, Changchun 130033, Jilin, China. E-mail: liuxy@ciomp.ac.cn
[d] Key Lab of Organic Optoelectronics and Molecular Engineering, Department of Chemistry, Tsinghua University, Beijing 100084, China

† Electronic supplementary information (ESI) available. See DOI: 10.1039/d0tc05391k

contribute to suppressing the energy transfer among QDs, resulting in an enhancement in the luminance efficiency.[23,24] However, the surface organic ligands typically used to stabilize QDs are long amphiphilic ligands (*e.g.*, oleic acid (OA), or oleylamine).[25] The long aliphatic ligands become an insulating layer in solid QD films and affect the charge injection into the QDs, leading to a low fraction of injected charges that form excitons and a poor device performance.

To solve this problem, capping ligand modified QDs were synthesized to enhance the EL performance of QLEDs. It is found that the functionalized ligands strengthen the molecular bonds between QDs, improving the QD passivation and stability.[24,26,27] Surface defects, imperfections in surface passivation, typically lead to midgap states, which results in weak or completely inactive lowest-energy optical transitions.[28] Otherwise, the surface chemistry, as well as the interparticle separation, plays a major role in controlling carrier transfer at the QD interface.[29] The valence state of QDs is strongly correlated with ligand molecules bound to the surface of nanocrystals. Ligand-induced QD optical band gap changes cause a shift of the valence band edge of the QDs.[30] Allowing for the potential barrier for electron or hole carriers and PL QY influenced by surface organic ligands, it is necessary to find suitable organic ligands for effective charge transport in QLEDs.

By replacing the conventional OA ligands on the as-synthesized QDs with shorter chain ligands, external quantum efficiency (EQE) over 10% of blue-violet QLEDs and EQE over 20% of green QLEDs were obtained.[31,32] In 2019, Y. Sun *et al.* improved the thermal stability of QDs by replacing the OA ligands with 1-dodecanethiol (DDT), and the green QLEDs exhibited a droop-free efficiency over a wide range of brightnesses.[33] The thiol anchor based QLEDs show important potential in long-lifetime devices for solid state lighting and display arrays. However, the maximum EQE of the best performance device is only 16.6%, which is lower than previous studies in the literature.[34,35] Despite its important potential, a systematic study on tailoring the thiol-based ligands of QDs in relation with the QLED performance is lacking. In this study, red QDs with shorter alkylthiols, DDT and 1-octanethiol (OT), were synthesized with partially replaced OA ligands to further improve the maximum luminance efficiency and operational lifetime. Devices based on OT-QDs showed an enhancement of the overall charge balance in the QLEDs and a maximum EQE of over 20%. And the best-performing QLED based on OT-QDs reached a maximum luminance of over 170 000 cd m^{-2} and 3.42-fold operational lifetime (421 000 h) enhancement compared to the reference one, DDT-based QLEDs (123 000 h).

Experimental details

Fabrication of QLEDs

The antireflection coating layer consisting of Ta_2O_5, SiO_2, and ITO films were deposited by electron beam evaporation under an oxygen pressure of 2.6×10^{-3} Pa and at deposition rates of 2, 4 and 3–4 Å s^{-1}, respectively. In order to achieve good light emission, the structure and thickness of the film are simulated to form an effective resonant cavity. The suitable structure of a multilayer is glass/$(Ta_2O_5/SiO_2)^6$/ITO, and the thickness of each layer is 76.78, 110.12 and 79.26 nm for Ta_2O_5, SiO_2, and ITO, respectively. The custom-made ITO electrodes with a similar sheet resistance to commercial ITO electrodes ($\sim$15 Ω $\square^{-1}$) were treated with the UV-ozone method for 15 min. The PEDOT:PSS (Baytron PVPAl 4083, filtered through a 0.22 μm filter) was spin-coated on the ITO electrodes at 2500 rpm for 40 s. Then the PEDOT:PSS-coated substrates were transferred into a nitrogen-filled glove box. PVK (8 mg ml^{-1}), QDs (10 mg ml^{-1}), and ZnMgO NPs (20 mg ml^{-1}) were deposited layer by layer by spin-coating on the PEDOT:PSS layer. The PVK, and ZnMgO layers were baked at 170 °C for 30 min and 110 °C for 10 min, respectively. The QD layer was spin-coated at 3500 rpm for 40 s. Finally, Al electrodes (100 nm) were deposited using a thermal evaporation system through a shadow mask under a high vacuum of 1×10^{-4} Pa.

Results and discussion

By partially replacing the OA ligands on the as-synthesized QDs with shorter thiol ligands, CdSe@ZnS QDs based on DDT and OT ligands (DDT-QDs and OT-QDs) were synthesized. The ligand exchange process is demonstrated in Fig. 1a and the detailed synthetic strategies are provided in the experimental part in the ESI.† The Fourier transform infrared (FTIR) spectra of QDs based on the replaced ligands are shown in Fig. S1 (ESI†). The greatly weakened stretching vibrations of C=O at 1544 and 1448 cm^{-1} compared with that of OA-QDs and the stretching vibration frequency of S–C at 722 cm^{-1} means that the OA ligands were successfully partially replaced by the thiol-ligands. ^{1}H NMR measurements were used to confirm the two kinds of ligands, as demonstrated in Fig. 1b. With similar molecular structures, the difference between DDT and OT is the alkyl chain length and the number of hydrogen atoms (the c-part of the molecular structure, inset in Fig. 1b). It can be seen that the integral area (c-H) of DDT is larger than that of OT. The calculated numbers of c-H atoms are 16.96 and 10.46 for DDT-QDs and OT-QDs, respectively, which coincide with the molecular structure. The combination of FTIR and ^{1}H NMR spectroscopic analysis suggests that the long chain OA ligands as formed in the synthesis process are successfully partially replaced by DDT or OT ligands. Fig. 1c and d show the transmission electron microscopy (TEM) images of DDT-QDs and OT-QDs, respectively. The average size of the OT-QDs (12.10 nm) is larger than that of the DDT-QDs (10.68 nm), both of which are larger than that of the OA-QDs (9.65 nm, Fig. S2, ESI†). As shown in the energy dispersive spectroscopy (EDS) measurements in Fig. S3 and Table S1 (ESI†), it noted that the S : Zn ratio is also improved from 0.86 : 1 to 0.93 : 1 after applying DDT and to 1 : 1 after applying OT, respectively. The large size QDs are probably obtained due to the adsorption of thiol ligands, which serve as an extra S source and promote the growth of a ZnS outer shell.[33] TEM images show

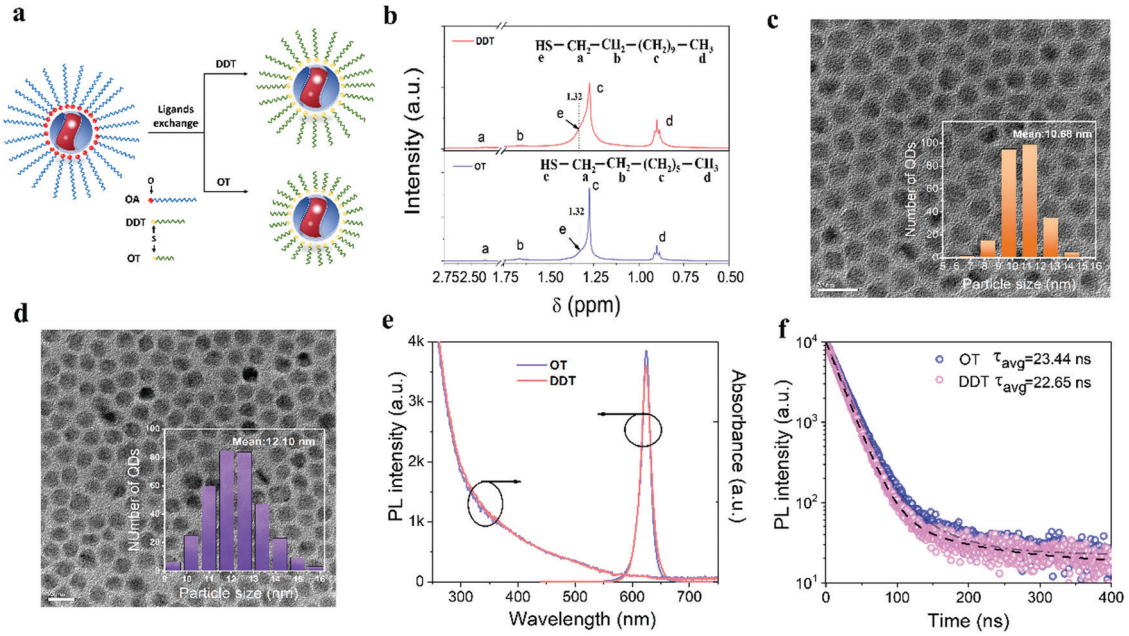

Fig. 1 (a) The ligand exchange strategy diagram of QDs. (b) ^{1}H NMR spectra of the QDs after ligand exchange with DDT (upper panel) and OT (lower panel). Inset: Molecular structure of DDT and OT. TEM images of (c) DDT-QD film and (d) OT-QD film. Inset: Corresponding size distribution. (e) UV-abs spectroscopy and PL spectra of QDs with different surface ligands. (f) Evolution of the PL decay curves of DDT-QD and OT-QD solution.

that both the DDT-QDs and OT-QDs achieve good monodispersivity properties.

Ultraviolet visible absorption (UV-abs) and photoluminescence (PL) spectra of the two kinds of QDs are shown in Fig. 1e. With a similar absorption edge, the OT-QD solution exhibits a strong red PL band at 624 nm with a full width at half-maximum (FWHM) of only 18 nm and PL QY of 80%, while the DDT-QD solution exhibits a lower peak emission at 624 nm with a quite narrow FWHM of 20 nm. By improving the QD passivation with shorter thiol-based ligands, the OT-QD film (20 nm) exhibits a higher PL QY of 75%, while the DDT-QD film gives 67%, both of which are higher than that of the OA-QD film (62%, Fig. S4, ESI†). The PL QY enhancement of the emitting layer (EML) caused by surface ligands could reflect a better EL performance of the OT-QD device. As the UV-abs spectra are similar and there is no peak shift of their PL band in Fig. 1e, the bandgaps of DDT-QDs and OT-QDs are assumed to be the same, ≈1.99 eV. The PL decay curves of DDT-QDs and OT-QDs in solution are exhibited in Fig. 1f, showing a decay of dual channel quenching. The average excited state lifetimes (τ_{avg}) of the QD solutions are extracted from the PL decay curves (Fig. S6 and Table S2, ESI†). Compared with the DDT-QD solution (22.65 ns), an enhanced PL lifetime of 23.44 ns is obtained for the OT-QD solution. A lifetime reduction in the solid state is observed in the 20 nm QD film (Fig. S7, ESI†). A relatively large τ_{avg} of 12.89 ns is obtained for the OT-QD film. Taking the suppressed nonradiative progress into account, the QDs with OT ligands reach stronger PL emission and longer excited state lifetimes. It can be seen that the strategy of using a shorter OT-ligand can improve QD passivation and stability, which can be verified by the decreased nonradiative decay rate from 3.03×10^{7} of the DDT-QD film to 1.66×10^{7} of the OT-QD film. The decreased nonradiative decay can be extracted by following the formulae, $\mathrm{PLQY} = \frac{k_r}{(k_r + k_{nr})}$ and $\tau_{avg} = \frac{1}{(k_r + k_{nr})}$. The shorter thiol-based ligands could help improve the QD passivation and OT-QDs reach a better optical performance.

In addition to their optical properties, the electronic properties of the QDs play an important role in determining the EL performance of QLEDs. In a previous work, D. F. Watson *et al.* characterized that electron transfer between tethered nanoparticles as a function of the interparticle separation by varying the alkyl chain length.[36] Short chain ligands are selected to decrease the width of inter-QD barriers and produce a conductive film[37] by decreasing the inter-QD distance (Fig. 2a). The effective channels for tunneling[38] are facilitated by the strong coupling between the overall shorter ligands and the ligand orbitals in a QD aggregate film. The band edge energies can be tuned by passivating the surface with dipolar ligands.[39] To investigate the surface ligand effect on the energy band structure of the QD films for LEDs, ultraviolet photoelectron spectroscopy (UPS) was performed using a Thermo ESCALAB 250 surface analysis system with a monochromatic He I light source (21.2 eV). As shown in the UPS spectra (Fig. 2b), the high-binding energy cutoff (E_{cutoff}) of the QDs changes as the surface ligand varies, as well as the onset energy in the valence-band edge (E_{onset}) regions. The E_{onset} values for OT and DDT capped QD films are 2.03 eV and 2.24 eV, respectively. The valence band levels (E_v) of the OT-QD and DDT-QD surface ligands are calculated according to the equation VBM = 21.2 − (E_{cutoff} − E_{onset}), and are −6.59 and −6.70 eV, respectively. Ligand modification makes OT-QDs behave with a higher VBM level. Allowing for the similar bandgaps (≈1.99 eV) obtained

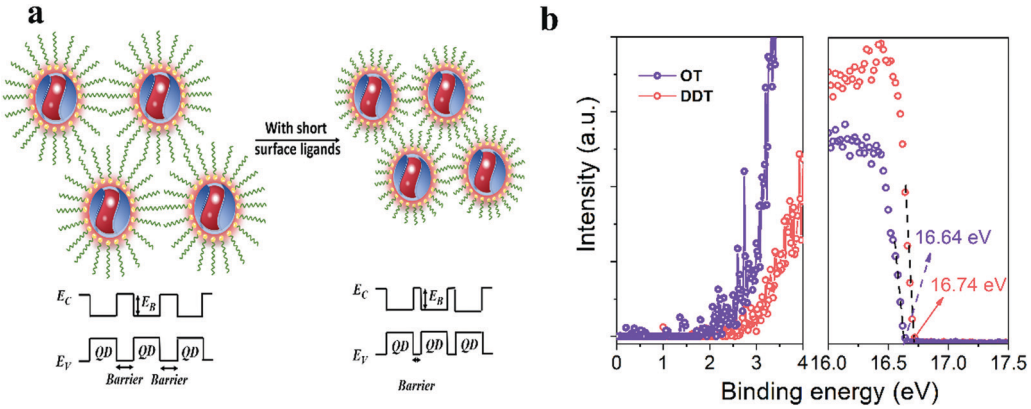

Fig. 2 (a) The illustration of short chain based QDs. (b) UPS spectra of QDs with different surface ligands.

from the UV-abs spectroscopy, the conduction band levels (E_c) of these two QDs are determined to be −4.60 and −4.71 eV, respectively.

The conventional hybrid structure of the representative QLEDs is demonstrated in Fig. 3a. The multiple layers are indium tin oxide (ITO), poly(ethylenedioxythiophene):polystyrene (PEDOT:PSS, 25 nm), poly(9-vinlycarbazole) (PVK, 30 nm), QDs (20 nm), ZnMgO nanoparticles (NPs, 30 nm), and aluminum (Al, 100 nm). The PVK layer is used as the hole transport layer (HTL) to reduce the hole injection barrier at the HTL/EML interface. According to the reported literature[40,41] and our previous work,[42] the $Zn_{0.85}Mg_{0.15}O$ NPs (Fig. S8, ESI†) are used as transport materials in this work, which can serve as the electron transport layer and reduce the electronic current of the devices. The cross-section scanning electron microscopy (SEM) image of QLEDs is exhibited in Fig. 3b, showing the direct contact interfaces in the device. The energy level diagram of QLEDs with different emitting layers is shown in Fig. 3c. It is observed that the potential barrier between the PVK layer and the OT-QD emitting layer is 0.11 eV lower than that between the HTL and the DDT-QD layer, and thus the hole could be facilitated to transport and inject into the EML.

For the purpose of comparing the carrier transport and injection characteristics of OT and DDT capped QDs, hole-only and electron-only devices were fabricated and the current density–voltage (J–V) properties were collected. The multiple layers of the hole-only device (inset in Fig. 3d) are ITO/PEDOT:PSS (20 nm)/PVK (30 nm)/QDs (20 nm)/MoO_x (30 nm)/Al (100 nm), where the MoOx is used to block the hole injection from the electrodes. The represented electron-only device of ITO/ZnMgO (30 nm)/QDs (20 nm)/ZnMgO (30 nm)/Al (100 nm) is shown in Fig. 3e, and the two ZnMgO NP layers block the hole injection from the electrodes. As the J–V curve of the

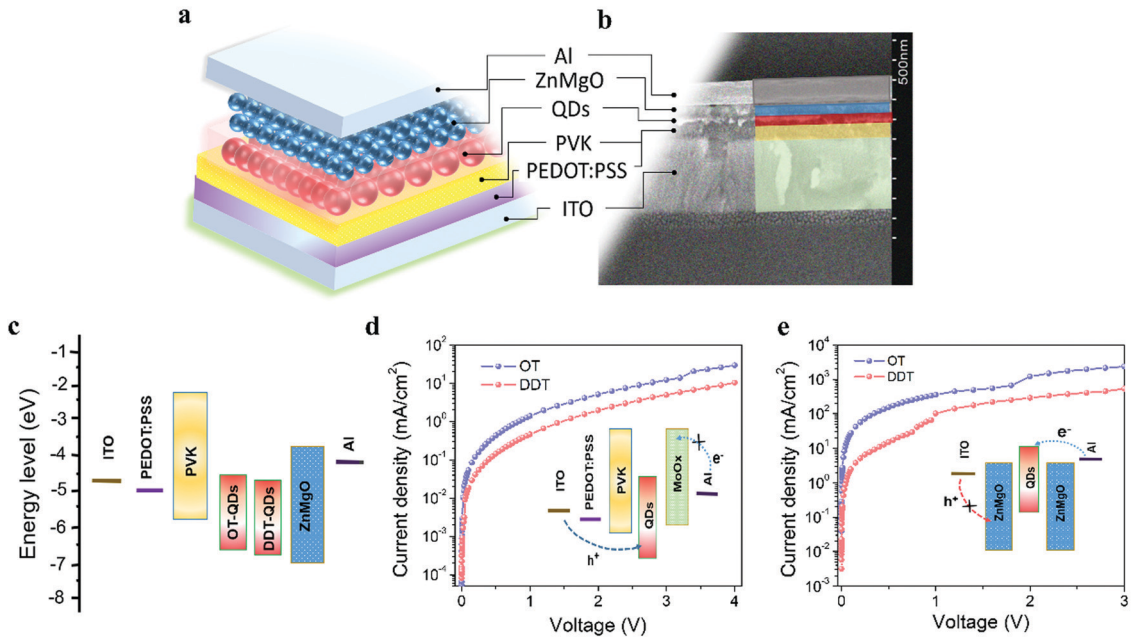

Fig. 3 (a) Schematic illustration and (b) cross-sectional SEM image of QLEDs. (c) Energy level diagram of multiple layers in QLEDs. Current density–voltage curves of (d) hole-only and (e) electron-only devices based on different QD films.

electron device in Fig. 3d shows, the current density of the OT-QD based hole-only devices is 3.5-fold higher than that of the DDT-QD based devices. Due to the reduction of the potential barrier, the current density of both the hole-only and electron-only device based on the OT-QDs is larger than that of the DDT-QD based devices. Such exchange of surface shorter ligands results in greater current injection into the emitting QD layer. Thus, the exciton fraction of injected charges is enhanced, which could improve the overall charge balance in QLEDs.

Fig. 4 shows the EL properties of the best-performance QLEDs based on OT-QDs and DDT-QDs. Normalized EL spectra of QLEDs are presented in Fig. 4a; the emission peak of QLEDs based on DDT-QDs is 628 nm with a FWHM of 22 nm, corresponding to Commission International de I'Eclairage (CIE) 1931 color coordinates of (0.686, 0.312, Fig. S9a, ESI†). However, for QLEDs based on OT-QDs, the peak wavelength of the EL spectrum is 630 nm with a FWHM of 24 nm corresponding to the CIE 1931 color coordinates of (0.690, 0.310). Compared with the PL spectra in Fig. 1e, EL emission peaks of traditional QLEDs typically exhibit 4–6 nm red shifts and 4 nm broadened FWHMs, owing to the quantum-confined Stark effect and larger exciton polarization under a higher electric field, resulting in the increased LO (longitudinal optical)–phonon coupling.[43–46] Fig. 4b demonstrates the current density–voltage–luminance (J–V–L) characteristics of QLEDs. With a low hole injection barrier, a larger current density is obtained for the device based on OT-QDs (device A). A maximum L of 137 000 cd m^{-2} is obtained for the device based on DDT-QDs (device B) at a driving voltage of 11.6 V, while a higher L of 171 000 cd m^{-2} is achieved for device A at a driving voltage of 10.8 V. CE and EQE curves are exhibited in Fig. 4c. A quite high maximum CE of 23.9 cd A^{-1}, corresponding to an EQE of 16.8%, is achieved for device B at a L value of 49 600 cd m^{-2}. Due to the high PL properties and high VBM level of OT-QDs (Fig. 2), device A reaches an approximately 1.5-fold higher maximum CE of 35.5 cd A^{-1} at a current density of 41.6 mA cm^{-2}. Device A reaches a maximum EQE of 25.1% at a L value of 14 800 cd m^{-2}. The luminance efficiency shows a low efficiency roll-off and the CE remained 90% at L over 62 000 cd m^{-2} (Fig. S11, ESI†). As the histograms for 28 devices from five batches in Fig. S12 (ESI†) show, the high average peak EQE, 20.77%, is encouraging.

Why can this happen in such devices for same size QDs with varied chain length ligands on the QDs? The ligand effect is vital for the device performance. The ligand introduces two effects on the QD film in the device as shown in Fig. S9b (ESI†). (1) The ligand plays a role in the confinement barrier with a high bandgap; whatever its carbon chain length is, it can confine the carriers within the QDs in solution to protect the exciton from quenching and this is a crucial effect for the highly efficient exciton recombination. That is why the OT and DDT can give a similar emission PL QY. (2) There is interfacial polaron formation on the carbon chain after the photoexcitation of such QDs,[38] which can facilitate the carrier transport or injection in the carbon chain. This polaron occurs in the carbon chain near the thiol group side of the ligand, which may be enhanced for the condensation situation in the QD film. For the QD aggregates, their electronic state can be coupled to form a new state[47,48] if they become close enough, which will influence the individual QD emission. In the OT capped films, OT molecules supplied enough confinement distance to protect the QD aggregation or quenching, but present enough distance for polaron assisted electronic injection into the QDs for emission. This can be evidenced from the band structure data

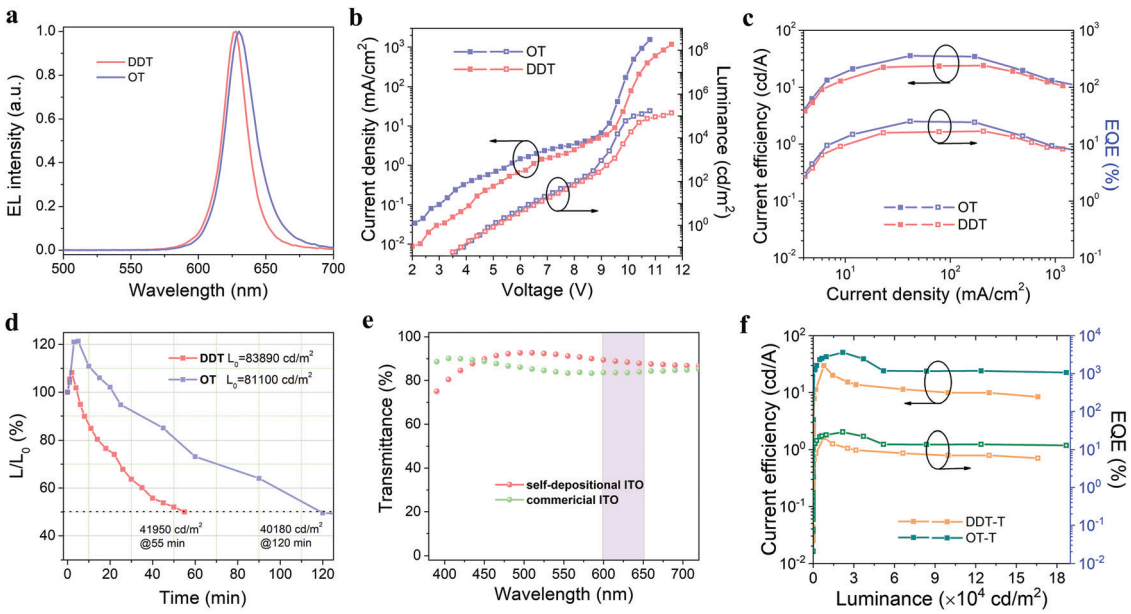

Fig. 4 EL performance of QLEDs based on OT-QDs and DDT-QDs: (a) normalized EL spectra. (b) J–V–L characteristics. (c) CE and EQE curves as a function of current density. (d) Operational lifetime. (e) Transmittance of commercial ITO and self-depositional ITO film. (f) CE and EQE characteristics of devices based on self-depositional ITO electrodes.

Table 1 Summary of wavelength (λ_{max}) and FWHM of EL peak, EQE at L of 10 000 cd m^{-2}, maximum CE (CE_{max}), maximum EQE (EQE_{max}) and maximum L (L_{max}) of QLEDs

Device	λ_{max} (nm)	FWHM (nm)	CE_{max} (cd A^{-1})	EQE @ L of 10 000 cd m^{-2}	EQE_{max} (%)	L_{max} (cd m^{-2})
A	630	24	35.5	20.1	25.1	171 000
B	628	22	23.9	16.1	16.8	137 000
A–T	630	24	50.7	24.3	29.0	187 000
B–T	628	22	33.3	19.0	20.9	166 000

($E_g \approx 1.99$ eV) in Fig. 2b, which are very close to the naked individual QD. This indicates that the confinement energy and polaron energy cancel with each other, this facilitates the injection of electron and holes into QDs. For the DDT capped QD film, the UPS band edge moves to 2.24 eV. This indicates that the DDT molecules supplied a 0.21 eV larger confinement energy, which presented a higher band barrier blocking the electron or hole injection into the QD film. That is why the data showed up in Fig. 3d and e and 4b. Finally, they produce the EL performance differences in Fig. 4.

To investigate the operational lifetime of the QLEDs, stability measurements were conducted under ambient conditions (indoor temperature, 25 °C, relative humidity, 40–60%). At a constant current density, device A is tested at an initial L of 81 100 cd m^{-2}, while the initial L of device B is 83890 cd m^{-2}. The operational lifetime (T_{50}) is defined as the time required for a 50% decrease of the initial luminance as shown in Fig. 4d. With an acceleration factor of 1.83 (Fig. S15, ESI†), the T_{50} for device A at a display-relevant L of 100 cd m^{-2} is 421 000 h, which is over 3.42-fold larger than that of device B (123 000 h). For bottom emission QLEDs, the low transmission of the bottom substrate affects the light out-coupling efficiency, resulting in poor EL performance. To further enhance the luminance efficiency of QLEDs, an ITO substrate with a high transmittance film is deposited and used as an electrode; the detailed depositional information is provided in the Experimental part. The transmittance spectra of different ITO films are demonstrated in Fig. 4e. Compared with the commercial ITO film, the self-depositional one reaches a higher transmittance at the range from 500 to 650 nm, covering the red emission wavelength of this work. Due to the increase of transmission, maximum brightnesses of devices based on OT-QDs and DDT-QDs are obtained with ~20 000 cd m^{-2} enhancement (Table 1). As a result, simultaneous enhancement of CE and EQE are all achieved as shown in Fig. 4f. Device B based on a self-depositional ITO substrate (device B–T) reaches a maximum CE of 29.6 cd A^{-1} at a current density of 5.32 mA cm^{-2}, corresponding to a maximum EQE of 20.9%. While for self-depositional ITO substrate-based device A (device A–T), a higher maximum EQE of 29%, corresponding to a maximum CE of 50.7 cd A^{-1}, is achieved at a L of 21 800 cd m^{-2}. To our knowledge, the highest 29% EQE of the QLED can be compared to the record result.[49] Taking the device with or without a self-depositional ITO substrate into account, it is obvious that shorter OT ligand passivated QDs are an efficient method to achieve an efficient device with high luminance efficiency and long operational lifetime.

Conclusions

In summary, we have demonstrated an efficient strategy for realizing high luminance efficiency QLEDs by using shorted alkylthiols (OT) as a surface ligand on QDs. The exchange of surface ligands can improve the stability of QDs. Compared with the reference DDT-QD film, a higher PL QY is achieved for the OT-QD film. Moreover, the OT-QD film exhibits a higher valence band level, and a lower hole injection barrier. And holes are facilitated to transport and inject into the EML, thus improving the overall charge balance in QLEDs. An enhanced EQE of 25.1% is obtained for devices based on OT-QDs while the device based on DDT-QDs reaches a maximum EQE of 16.8%. As a result, the operational lifetime T_{50} at a luminance of 100 cd m^{-2} obtained a 3.42-fold improvement for device A of 421 000 h. OT-ligand exchange is an excellent method to enhance the stability and luminance efficiency of QLEDs. To further improve the EL performance, a higher transmission self-depositional ITO film is used as the electrode, and a maximum 29% EQE is obtained for QLEDs based on OT-QDs. This work highlights the potential of thiol-based ligands as the surface ligands in constructing stable QDs and high-performance QLEDs. We believe that this will open up a new opportunity for long lifetime QLEDs in their application to solid-state lighting and display arrays.

Conflicts of interest

The authors declare no competing financial interest.

Acknowledgements

This work was funded by the China Postdoctoral Science Foundation (2019M653808XB); the National Natural Science Foundation of China (11774134, 61975256, 51973208, 61774154 and 61875195); the 2018 Guangxi Post-Doctoral Innovative Talent Support Program; the special funding of ''Guangxi Bagui Scholar''; the Jilin Province Science and Technology Research Project (20190302087GX, and 20190302084GX); the National Key Research and Development Program of China (2016YFB0401701); the Open Fund of the State Key Laboratory of Luminescent Materials and Devices (South China University of Technology, 2019-skllmd-07); Open Project of the State Key Laboratory of Luminescence and Applications (SKLA-Z-2020-01), and the Cooperation Fund between CIOMP and FuDan University.

References

1 X. Li, Q. Lin, J. Song, H. Shen, H. Zhang, L. S. Li, X. Li and Z. Du, Quantum-Dot Light-Emitting Diodes for Outdoor

Displays with High Stability at High Brightness, *Adv. Opt. Mater.*, 2020, **8**(2), 1901145.

2 J. Song, O. Wang, H. Shen, Q. Lin and L. S. Li, Quantum Dot LEDs: Over 30% External Quantum Efficiency Light-Emitting Diodes by Engineering Quantum Dot-Assisted Energy Level Match for Hole Transport Layer, (Adv. Funct. Mater. 33/2019), *Adv. Funct. Mater.*, 2019, **29**(33), 1970226.

3 C. Dang, J. Lee, C. Breen, J. S. Steckel, S. Coe-Sullivan and A. Nurmikko, Red, Green and Blue Lasing Enabled by Single-Exciton Gain in Colloidal Quantum Dot Films, *Nat. Nanotechnol.*, 2012, **7**(5), 335–339.

4 Y. Li, F. Yang, Y. Wang, G. Shi, Y. M. Maung, J. Yuan, S. Huang and W. Ma, Magnetron Sputtered SnO_2 Constituting Double Electron Transport Layers for Efficient PbS Quantum Dot Solar Cells, *Sol. RRL*, 2020, **4**(7), 2000218.

5 F. Ma, C.-C. Li and C.-Y. Zhang, Development of Quantum Dot-based Biosensors: Principles and Applications, *J. Mater. Chem. B*, 2018, **6**(39), 6173–6190.

6 H. Zhang, X. Ma, Q. Lin, Z. Zeng, H. Wang, L. S. Li, H. Shen, Y. Jia and Z. Du, High-Brightness Blue InP Quantum Dot-Based Electroluminescent Devices: The Role of Shell Thickness, *J. Phys. Chem. Lett.*, 2020, **11**(3), 960–967.

7 C. Pu, X. Dai, Y. Shu, M. Zhu, Y. Deng, Y. Jin and X. Peng, Electrochemically-Stable Ligands Bridge the Photoluminescence-Electroluminescence Gap of Quantum Dots, *Nat. Commun.*, 2020, **11**(1), 937.

8 Y. Yang, Y. Zheng, W. Cao, A. Titov, J. Hyvonen, J. R. Manders, J. Xue, P. H. Holloway and L. Qian, High-Efficiency Light-Emitting Devices based on Quantum Dots with Tailored Nanostructures, *Nat. Photonics*, 2015, **9**(4), 259–266.

9 Y. Shirasaki, G. J. Supran, M. G. Bawendi and V. Bulović, Emergence of Colloidal Quantum-Dot Light-Emitting Technologies, *Nat. Photonics*, 2012, **7**(1), 13–23.

10 K.-H. Lee, J.-H. Lee, H.-D. Kang, B. Park, Y. Kwon, H. Ko, C. Lee, J. Lee and H. Yang, Over 40 cd A^{-1} Efficient Green Quantum Dot Electroluminescent Device Comprising Uniquely Large-Sized Quantum Dots, *ACS Nano*, 2014, **8**(5), 4893–4901.

11 B. N. Pal, Y. Ghosh, S. Brovelli, R. Laocharoensuk, V. I. Klimov, J. A. Hollingsworth and H. Htoon, 'Giant' CdSe/CdS Core/Shell Nanocrystal Quantum Dots as Efficient Electroluminescent Materials: Strong Influence of Shell Thickness on Light-Emitting Diode Performance, *Nano Lett.*, 2011, **12**(1), 331–336.

12 C. Ikjun, J. Heeyoung, J. B. Guk, H. Donghyo, J. H. Chang, L. Taesoo, C. Kookheon, D. C. Lee, L. Jaehoon and L. Changhee, Ligand-Asymmetric Janus Quantum Dots for Efficient Blue-Quantum Dot Light-Emitting Diodes, *ACS Appl. Mater. Interfaces*, 2018, **10**(26), 22453–22459.

13 Z. Bao, Z.-F. Jiang, Q. Su, H.-D. Chiu, H. Yang, S. Chen, R.-J. Chung and R.-S. Liu, ZnSe:Te/ZnSeS/ZnS Nanocrystals: an Access to Cadmium-Free Pure-Blue Quantum-Dot Light-Emitting Diodes, *Nanoscale*, 2020, **12**(21), 11556–11561.

14 J. Kwak, J. Lim, M. Park, S. Lee, K. Char and C. Lee, High-Power Genuine Ultraviolet Light-Emitting Diodes Based On Colloidal Nanocrystal Quantum Dots, *Nano Lett.*, 2015, **15**(6), 3793–3799.

15 A. M. Dennis, B. D. Mangum, A. Piryatinski, Y. S. Park, D. C. Hannah, J. L. Casson, D. J. Williams, R. D. Schaller, H. Htoon and J. A. Hollingsworth, Suppressed Blinking and Auger Recombination in Near-Infrared Type-II InP/CdS Nanocrystal Quantum Dots, *Nano Lett.*, 2012, **12**(11), 5545–5551.

16 D. Chen, F. Zhao, H. Qi, M. Rutherford and X. Peng, Bright and Stable Purple/Blue Emitting CdS/ZnS Core/Shell Nanocrystals Grown by Thermal Cycling Using a Single-Source Precursor, *Chem. Mater.*, 2010, **22**(4), 1437–1444.

17 W. K. Bae, Y. S. Park, J. Lim, D. Lee, L. A. Padilha, H. McDaniel, I. Robel, C. Lee, J. M. Pietryga and V. I. Klimov, Controlling the Influence of Auger Recombination on the Performance of Quantum-Dot Light-Emitting Diodes, *Nat. Commun.*, 2013, **4**, 2661.

18 J. Lim, B. G. Jeong, M. Park, J. K. Kim, J. M. Pietryga, Y. S. Park, V. I. Klimov, C. Lee, D. C. Lee and W. K. Bae, Influence of Shell Thickness on the Performance of Light-Emitting Devices based on CdSe/Zn1-X CdX S Core/Shell Heterostructured Quantum Dots, *Adv. Mater.*, 2014, **26**(47), 8034–8040.

19 D. Bozyigit, O. Yarema and V. Wood, Origins of Low Quantum Efficiencies in Quantum Dot LEDs, *Adv. Funct. Mater.*, 2013, **23**(24), 3024–3029.

20 Y. Shirasaki, G. J. Supran, W. A. Tisdale and V. Bulović, Origin of Efficiency Roll-Off in Colloidal Quantum-Dot Light-Emitting Diodes, *Phys. Rev. Lett.*, 2013, **110**(21), 217403.

21 N. C. Anderson, M. P. Hendricks, J. J. Choi and J. S. Owen, Ligand Exchange and the Stoichiometry of Metal Chalcogenide Nanocrystals: Spectroscopic Observation of Facile Metal-Carboxylate Displacement and Binding, *J. Am. Chem. Soc.*, 2013, **135**(49), 18536–18548.

22 Y. Liu, J. Tolentino, M. Gibbs, R. Ihly and M. Law, PbSe Quantum Dot Field-Effect Transistors with Air-Stable Electron Mobilities above 7 $cm^2 V^{-1} s^{-1}$, *Nano Lett.*, 2013, **13**(4), 1578–1587.

23 I. Cho, H. Jung, B. G. Jeong, J. H. Chang, Y. Kim, K. Char, D. C. Lee, C. Lee, J. Cho and W. K. Bae, Multifunctional Dendrimer Ligands for High-Efficiency, Solution-Processed Quantum Dot Light-Emitting Diodes, *ACS Nano*, 2017, **11**(1), 684–692.

24 Y.-H. Won, O. Cho, T. Kim, D.-Y. Chung, T. Kim, H. Chung, H. Jang, J. Lee, D. Kim and E. Jang, Highly Efficient and Stable InP/ZnSe/ZnS Quantum Dot Light-Emitting Diodes, *Nature*, 2019, **575**(7784), 634–638.

25 D. V. Talapin, J.-S. Lee, M. V. Kovalenko and E. V. Shevchenko, Prospects of Colloidal Nanocrystals for Electronic and Optoelectronic Applications, *Chem. Rev.*, 2010, **110**(1), 389–458.

26 P. R. Brown, D. Kim, R. R. Lunt, N. Zhao, M. G. Bawendi, J. C. Grossman and V. Bulović, Energy Level Modification in Lead Sulfide Quantum Dot Thin Films through Ligand Exchange, *ACS Nano*, 2014, **8**(6), 5863–5872.

27 A. H. Ip, S. M. Thon, S. Hoogland, O. Voznyy and E. H. Sargent, Hybrid Passivated Colloidal Quantum Dot Solids, *Nat. Nanotechnol.*, 2012, **7**(9), 577–582.

28 S. V. Kilina, P. K. Tamukong and D. S. Kilin, Surface Chemistry of Semiconducting Quantum Dots: Theoretical Perspectives, *Acc. Chem. Res.*, 2016, **49**(10), 2127–2135.

29 D. A. Hines and P. V. Kamat, Quantum Dot Surface Chemistry: Ligand Effects and Electron Transfer Reactions, *J. Phys. Chem. C*, 2013, **117**(27), 14418–14426.

30 C. Giansante, Surface Chemistry Control of Colloidal Quantum Dot Band Gap, *J. Phys. Chem. C*, 2018, **122**(31), 18110–18116.

31 H. Shen, W. Cao, N. T. Shewmon, C. Yang, L. S. Li and J. Xue, High-Efficiency, Low Turn-On Voltage Blue-Violet Quantum-Dot-based Light-Emitting Diodes, *Nano Lett.*, 2015, **15**(2), 1211–1216.

32 H. Moon and H. Chae, Efficiency Enhancement of All-Solution-Processed Inverted-Structure Green Quantum Dot Light-Emitting Diodes Via Partial Ligand Exchange with Thiophenol Derivatives Having Negative Dipole Moment, *Adv. Opt. Mater.*, 2019, **8**(1), 1901314.

33 Y. Sun, Q. Su, H. Zhang, F. Wang, S. Zhang and S. Chen, Investigation on Thermally Induced Efficiency Roll-Off: Toward Efficient and Ultrabright Quantum-Dot Light-Emitting Diodes, *ACS Nano*, 2019, **13**(10), 11433–11442.

34 M. Zhang, B. Hu, L. Meng, R. Bian, S. Wang, Y. Wang, H. Liu and L. Jiang, Ultrasmooth Quantum Dot Micropatterns by a Facile Controllable Liquid-Transfer Approach: Low-Cost Fabrication of High-Performance QLED, *J. Am. Chem. Soc.*, 2018, **140**(28), 8690–8695.

35 H. Shen, Q. Gao, Y. Zhang, Y. Lin, Q. Lin, Z. Li, L. Chen, Z. Zeng, X. Li, Y. Jia, S. Wang, Z. Du, L. S. Li and Z. Zhang, Visible Quantum Dot Light-Emitting Diodes with Simultaneous High Brightness and Efficiency, *Nat. Photonics*, 2019, **13**(3), 192–197.

36 R. S. Dibbell and D. F. Watson, Distance-Dependent Electron Transfer in Tethered Assemblies of CdS Quantum Dots and, *J. Phys. Chem. C*, 2012, **113**(8), 3139–3149.

37 Y. Liu, M. Gibbs, C. L. Perkins, J. Tolentino, M. H. Zarghami, J. Bustamante, Jr and M. Law, Robust, Functional Nanocrystal Solids by Infilling with Atomic Layer Deposition, *Nano Lett.*, 2011, **11**(12), 5349–5355.

38 Y. Guo, F. Yang, X. Zheng, J. Tang, H. Zhong, A. Yu, J. Wang and B. Zou, Direct Observation of Surface Polarons in Capped CuInS2 Quantum Dots by Ultrafast Pump-Probe Spectroscopies, *J. Phys. Chem. Lett.*, 2019, **10**(18), 5297–5301.

39 S. Yang, D. Prendergast and J. B. Neaton, Tuning Semiconductor Band Edge Energies for Solar Photocatalysis Via Surface Ligand Passivation, *Nano Lett.*, 2012, **12**(1), 383–388.

40 H. C. Wang, H. Zhang, H. Y. Chen, H. C. Yeh, M. R. Tseng, R. J. Chung, S. Chen and R. S. Liu, Cadmium-Free InP/ZnSeS/ZnS Heterostructure-Based Quantum Dot Light-Emitting Diodes with a ZnMgO Electron Transport Layer and a Brightness of Over 10 000 cd m^{-2}, *Small*, 2017, **13**(13), 1603962.

41 M. Chrzanowski, M. Kuchowicz, R. Szukiewicz, P. Sitarek, J. Misiewicz and A. Podhorodecki, Enhanced Efficiency of Quantum Dot Light-Emitting Diode by Sol–Gel Derived $Zn_{1-x}Mg_xO$ Electron Transport Layer, *Org. Electron.*, 2020, 105656.

42 L. Wang, J. Lin, X. Liu, S. Cao, Y. Wang, J. Zhao and B. Zou, Mg-Doped ZnO Nanoparticle Films as the Interlayer between the ZnO Electron Transport Layer and InP Quantum Dot Layer for Light-Emitting Diodes, *J. Phys. Chem. C*, 2020, **124**(16), 8758–8765.

43 P. O. Anikeeva, J. E. Halpert, M. G. Bawendi and V. Bulovic, Quantum Dot Light-Emitting Devices with Electroluminescence Tunable Over the Entire Visible Spectrum, *Nano Lett.*, 2009, **9**(7), 2532–2536.

44 F. Zhang, S. Wang, L. Wang, Q. Lin, H. Shen, W. Cao, C. Yang, H. Wang, L. Yu and Z. Du, Super Color Purity Green Quantum Dot Light-Emitting Diodes Fabricated by Using CdSe/CdS Nanoplatelets, *Nanoscale*, 2016, **8**(24), 12182–12188.

45 V. I. Klimov, S. A. Ivanov, J. Nanda, M. Achermann, I. Bezel, J. A. McGuire and A. Piryatinski, Single-Exciton Optical Gain in Semiconductor Nanocrystals, *Nature*, 2007, **447**(7143), 441–446.

46 A. Piryatinski, S. A. Ivanov, S. Tretiak and V. I. Klimov, Effect of Quantum and Dielectric Confinement on the Exciton–Exciton Interaction Energy in Type II Core/Shell Semiconductor Nanocrystals, *Nano Lett.*, 2007, **7**(1), 108–115.

47 M. Bayer, P. Hawrylak, K. Hinzer, S. Fafard, M. Korkusinski, Z. R. Wasilewski, O. Stern and A. Forchel, Coupling and Entangling of Quantum States in Quantum Dot Molecules, *Science*, 2001, **291**(5503), 451–453.

48 L. Cao, Y. M. Miao, Z. B. Zhang, S. S. Xie, G. Z. Yang and B. S. Zou, Exciton Interactions in CdS Nanocrystal Aggregates in Reverse Micelle, *J. Mater. Chem.*, 2005, **123**(2), 978.

49 J. Song, O. Wang, H. Shen, Q. Lin and L. S. Li, Quantum Dot LEDs: Over 30% External Quantum Efficiency Light-Emitting Diodes by Engineering Quantum Dot-Assisted Energy Level Match for Hole Transport Layer (Adv. Funct. Mater. 33/2019), *Adv. Funct. Mater.*, 2019, **29**(33), 1970226.

